

# TEMPERATURE-INDUCED CHANGES IN PORE STRUCTURE AND CATALYTIC PERFORMANCE OF ALUMINUM OXIDE MEMBRANES

Anvar Khamidov<sup>1</sup>, Farhodjon Hoshimov<sup>2,3</sup>, Khakimjan Butanov<sup>3</sup>, Shavkat Mamatkulov<sup>3</sup>, Bahrom Umarov<sup>4</sup>, Dong Fang<sup>5</sup>, Mika Sillanpää<sup>6</sup>, Luca Pasquini<sup>7</sup>, Philippe Knauth<sup>7</sup>, Olim Ruzimuradov<sup>1,3,4\*</sup>

<sup>1</sup>Turin Polytechnic University in Tashkent, Kichik khalqa yoli 17, Tashkent 100095, Uzbekistan <sup>2</sup>Research Institute of renewable energy sources under Ministry of Energy of the Republic of Uzbekistan, Tashkent, Uzbekistan

<sup>3</sup>Institute of Material Science, Academy of Sciences of the Republic of Uzbekistan, Chingiz Aytmatov 2b, Tashkent 100084, Uzbekistan

<sup>4</sup>Department of Chemistry, National University of Uzbekistan, Vuzgorodok 15, Tashkent 100174, Uzbekistan <sup>5</sup>Faculty of Materials Science and Engineering, Kunming University of Science and Technology, Kunming 650093, PR China

<sup>6</sup>Department of Chemical Engineering, School of Mining, Metallurgy and Chemical Engineering, University of Johannesburg, P.O. Box 17011, Doornfontein 2028, South Africa

<sup>7</sup>Aix-Marseille University Madirel (UMR CNRS 7246) Campus Etoile-St Jérôme 13013 Marseille, France \*e-mail: <u>o.ruzimuradov@polito.uz</u>

Received 04.09.2024 Accepted 27.12.2024

Abstract. In this study, we synthesized nanostructured anodic aluminum oxide (AAO) membranes through the two-step anodization process using oxalic acid as the electrolyte. The main objective was to investigate how the electrolyte temperature influences the formation of pores in the AAO membranes. Key parameters, including pore diameter, interpore distance, thickness, and porosity, were measured and subjected to statistical analysis. The experimental results clearly demonstrated that under specified conditions involving temperatures at 5, 15 and 25 °C, an oxalic acid concentration of 0.3 M, and applied voltage of 55 V, we achieved the successful fabrication of well-ordered nanoporous aluminum oxide membranes. The scanning electron microscopy (SEM) technique was used to examine both the surface morphology and cross-sectional views of the anodic membranes. Additionally, we explored the catalytic properties of nickel and molybdenum-impregnated AAO in the hydrogenation reaction of certain alkenes (C6-C8) across a range of temperatures. In the process of converting alkenes to alkanes, our research demonstrated that the Ni/AAO catalyst exhibited activity at 200 °C, while the Ni-Mo/AAO catalyst began to activate at around 250 °C.

**Keywords:** anodic aluminum oxide (AAO), oxalic acid, porosity, pore diameter, interpore distance, hydrogenation.

DOI: 10.32737/2221-8688-2025-4-533-541

#### Introduction

Anodic aluminum oxide (AAO) has emerged as a compelling nanomaterial that has attracted significant research interest. The fabrication of porous alumina on silicon substrates for the synthesis of nanoengineered structures integrated with electronic and optoelectronic devices has been the subject of numerous investigations [1-3]. Previous studies have attempted to create nano-porous aluminum oxide films through anodic oxidation processes involving both acidic and alkaline solutions. However, these studies encountered challenges,

resulting in films with notable irregularities in their porosity [4].

In 1998, Masuda et al. achieved a breakthrough by generating a highly ordered hexagonal pore structure using a two-step anodization process based on pre-arranged macroscopic parameters [5, 6]. Two types of membranes were employed in their research, one fabricated in-house and the other commercially available, both with an average pore diameter of 100 nm but varying in interpore spacing and surface roughness [7]. To improve the

anodization process, researchers often use electrolytes at low temperatures (typically in the range of 0-5 °C) to mitigate the high current density resulting from oxide dissolution [8]. Systematic testing of aluminum anodization was performed varying current density, electrolyte temperature, concentration and mixing conditions in citric acid solutions [9]. Notably, one of the critical concerns was related to corrosion resistance, particularly in the surface layer of aluminum alloys used in these processes [10]. Additionally, the temperature difference between the aluminum substrate and the electrolyte plays a pivotal role by affecting the formation of well-ordered pore structures within nanoporous anodic alumina [11]. However, temperature and time changes do not affect the

interpore distance [12].

The primary objective of this study is to emphasize the significance of carefully tailoring synthesis parameters to suit specific application requirements. Our analysis delves into the interrelation among synthesis variables including electrolyte concentration, temperature, anodization voltage. We closely examine the time-dependent behavior of current density, and its impact on structural properties of AAO membranes. These characteristics predominantly encompass pore size, interpore spacing, pore density, and membrane thickness. Additionally, we investigate the catalytic activity of AAO membranes infused with nickel and molybdenum in the hydrogenation of certain alkenes (C6-C8) at various temperatures.

## **Experimental part**

*Materials.* In this study, we employed commercially available 99.995% pure aluminum sheets (Beantown Chemical) as our substrate material. These samples were prepared with dimensions of approximately 3 cm<sup>2</sup> in width and 0.2 mm in thickness. To protect the edges and preserve one of the surfaces, the samples were encased in commercial acrylic adhesive, leaving an exact 2 cm<sup>2</sup> area exposed for testing.

Synthesis of AAO Coatings. A 2×2 cm plate in size was cut out and subjected to electropolishing in a solution composed of HClO<sub>4</sub> and ethanol mixed in a 1:4 volume ratio. The electropolishing process was carried out at 15 V for a duration of 1 minute, with the temperature maintained at 5 °C. Subsequently, the two-step anodization was performed in a 0.3 M oxalic acid solution at 5-25 °C. In order to reduce the Joule heating effect, the anodizing process is carried out at a relatively low temperature  $(-5 \sim 15 \, ^{\circ}\text{C})$  [13]. A.A. Ayalew et al. [14] also investigated the influence of control electrode temperature in the range of 5-65°C on porous alumina layer growth on Al. The thickness of the porous AAO membrane film formed in oxalic acid electrolyte increased from 32.2 µm to 52.5 µm, and from 3.4 to 33 µm [8]. AAO formation was achieved through the utilization of potentiostat (Corrtest CS 350M, China) and a three-electrode electrochemical cell. In this setup, a platinum mesh was served as the counter electrode, the aluminum acted as the

working electrode, and Ag/AgCl functioned as the reference electrode. To gain the deeper insight into the anodizing process, chronoamperometric curves were recorded.

Anodic Oxidation. The membranes were made using a two-step anodic oxidation process, one/two/multi-step anodization [15], with the precise conditions depending on the chosen electrolyte, in this case, a 0.3 M oxalic acid solution. During the initial anodization step, the membrane was subjected to 50 V for a duration of 15 minutes. Subsequently, the oxide layer produced during the initial step was chemically etched by immersing the test piece in a solution consisting of 6 wt% phosphoric acid and 1.8 wt% chromic acid. This etching process lasted for 2 hours at a temperature of 60 °C. The second anodization step was carried out on the same substrate at 55 V continuing for 4 hours. In J. Kim's work, the optimal time for AAO removal was determined to be 6 hours [16]. A platinum mesh was used as cathode during this phase of the process.

**Morphological Characterization of Coatings.** The morphology and pore characteristics of the AAO membranes were examined using high-resolution field emission scanning electron microscopy (JSM-7001, JEOL, Japan) and scanning electron microscopy (SEM SUPRA 40, Carl Zeiss). Parameters such as the arrangement of porous structures, average pore diameter  $(\overline{dp})$ , interpore distance  $(\overline{di})$ , oxide

film thickness  $(\bar{e})$ , and porosity  $(\bar{P})$  were determined from SEM micrographs using Image J software [17-19].

Catalytic Activity. Catalysts based on AAO were prepared, and the hydrogenation of certain alkenes (C6-C8) was conducted following procedures outlined in our previous work [20]. In brief, to obtain Ni/AAO and Ni-Mo/AAO catalysts, AAO was dipped in solutions containing Ni(NO<sub>3</sub>)<sub>2</sub>·6H<sub>2</sub>O and

(NH<sub>4</sub>)<sub>6</sub>Mo<sub>7</sub>O<sub>24</sub>·4H<sub>2</sub>O at room temperature. After each impregnation cycle, the plate was washed in water, dried, and immersed in the solution once more. Subsequently, the plate was then annealed in air at 550 °C for 5 hours. Hydrogen for the hydrogenation reaction was generated using a hydrogen generator from the "Chromatek" company, and the hydrogenation process was analyzed via gas chromatography utilizing an HP-5MS column.

#### Results and discussion

The nanostructured oxide membranes synthesized through a two-stage anodic oxidation in a 0.3 M oxalic acid solution at

different temperatures were examined by SEM (Fig. 1).

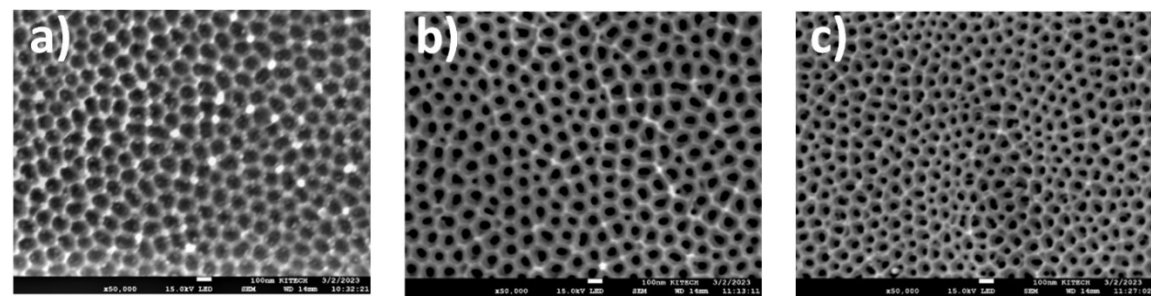


**Fig. 1.** SEM images of two-steps anodized porous AAO membranes. a) at 5 °C; b) at 15 °C and c) at 25 °C

The porosity of the AAO membrane synthesized through the two-stage anodic oxidation process, exhibits a temperature-dependent variation, as indicated in Figure 2. Specifically, the average pore diameter

 $\overline{dp}$  changes from 104 to 98 nm, while the poreto-pore distance extends to  $\overline{di}$  – 115 nm. The thickness of the oxide layer  $\overline{e}$  – varies between 14.4 and 30.2 µm and the degree of porosity  $\overline{P}$  – fluctuates from 26.8 to 32.2%.

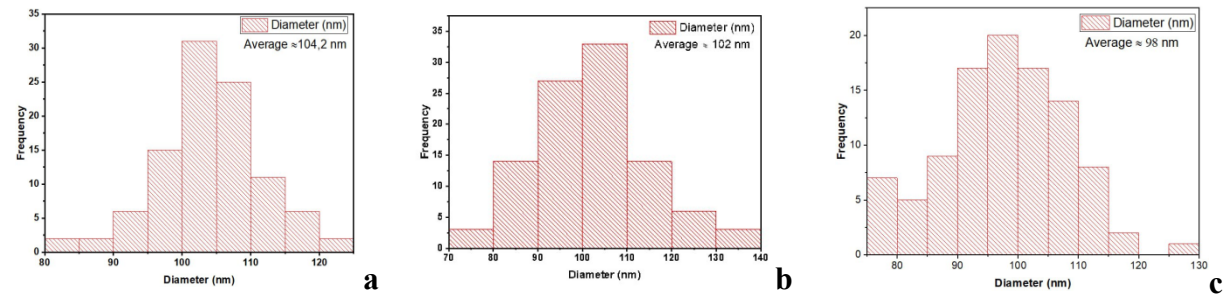


**Fig. 2.** Average values of the morphological parameters of nanostructured anodic aluminum oxide coatings obtained in oxalic acid as a function of temperature (a-5, b-15 and c-25 °C).

The optimal parameters of the AAO membranes obtained through the two-stage anodizing process are indicated by a special code, where "C0.3" represents the electrolyte concentration, "T15" signifies the electrolyte temperature, and "V55" corresponds to the anodizing voltage. Following the two-steps

anodizing, the pores in the porous AAO membrane were organized, resulting in porous membranes with expanded dimensions and a flat surface.

**AAO** pore diameter. The pore diameter of aluminum oxide during the anodization is mainly influenced by the choice of electrolyte and the

anodizing voltage, with minimal dependence on the duration of the oxidation time [21]. The pore diameter of the resulting from the anodic oxidation of aluminum was assessed in relation to the anodizing process parameters, including anode voltage, electrolyte concentration and temperature (Fig. 3). The experimental findings from anodic oxidation of aluminum in 0.3 M oxalic acid electrolytes showed that pore diameter of the AAO membrane remained unaffected by variations in the electrolyte temperature had almost no effect on the pore diameter of the AAO membrane.

It was also found that the anodizing temperature had a negligible effect on the pore diameter of the AAO membrane. Conversely, the study indicated that the anodizing temperature showed only a slight influence on the interpore distance. Over a temperature range from 5 to 25 °C, researchers observed a reduction in pore distance from 104 to 98 nm.

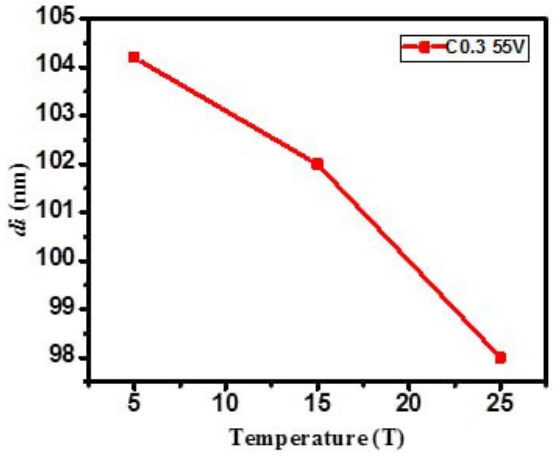


**Fig. 3.** Relationship between the average pore distance of nanostructured aluminum oxide membranes and the temperature of the electrolyte during the anodization process.

Thickness of the oxide layer. The thickness of the oxide layer was examined for sample T5

using both optical microscopy and SEM, as shown in Fig. 4.

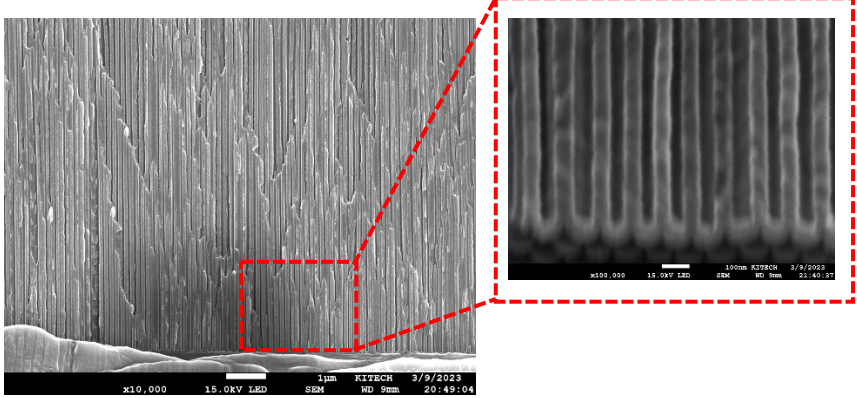


**Fig. 4.** Cross-sectional SEM image of the AAO film synthesized in two anodization steps at 5 °C and 55 V for 4 h.

To understand the effect of anodization process parameters on the thickness of the AAO additional investigations surface. were conducted. The findings revealed a clear relationship between higher electrolyte temperatures and increased thickness of the oxide layer. In particular, when the anodization was carried out at 5 °C, the oxide layer thickness

measured around 14.4  $\mu$ m, whereas at 25 °C, it expanded to approximately 30.2  $\mu$ m.

Additionally, the average porosity level of the AAO membrane formed through the anodic oxidation of aluminum was studied in relation to temperature variations. The anodization process yielded porous AAO membranes with an average porosity ranging from 26.8 to 32.2%. A

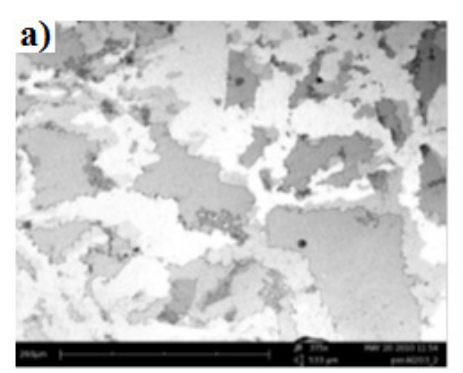
maximum in the average porosity was observed at 15 °C.

According to Nielsch et al. [19], it is stated that a porosity of approximately 10% is essential to achieve a self-ordering regulation of the porous matrix, regardless of anodization conditions. However, our anodization conditions did not result in a 10% porosity, a 25% porosity [22-24] as illustrated in Fig. 2.

In accordance with K. Chernyakova et al. [9], the rate of chemical dissolution of the barrier layer and pore walls did not depend on the anode temperature, however at an anodization

temperature 60 °C, the diameter of the holes increased by 1.7 times.

An equally important parameter during the anodization of aluminum film is temperature. Elevated temperature can lead to inhomogeneous and intense surface etching (Fig. 5 a). In this regard, the capability to regulate temperature during electrochemical processes holds significant importance. The higher voltage is needed to obtain a porous structure, maintaining a lower the electrolyte temperature becomes crucial. This approach enhances the selectivity of the electrochemical etching process.



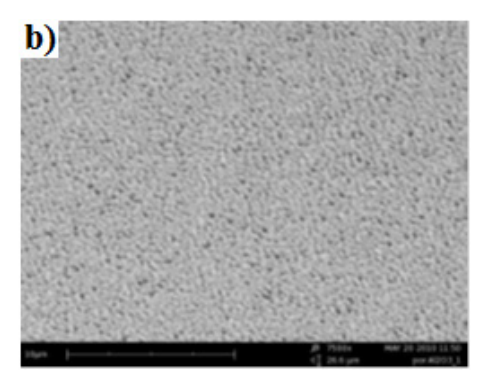


Fig. 5. Optical and SEM images of AAO (a) without and (b) with cooling

Comparing the results of AAO formation without cooling and with cooling under otherwise identical conditions, it becomes evident that the porous layers obtained with controlled low temperatures exhibit uniformity and clear boundaries, as shown in Fig. 5b.

Catalytic activity. Catalytic activity is a critical factor in determining the efficiency of nanoparticle containing catalysts. The size, texture, structural properties, and electronic state of atoms all exert significant influence on their catalytic performance and selectivity. It is worth noting that the size-dependent selectivity in the hydrogenation of monosubstituted disubstituted double bonds is prominently affected the diameter catalytic by of nanoparticles. This applies whether these nanoparticles are suspended or deposited onto micrometer-sized alumina substrates. A highly promising catalyst support is AAO, designed as platelets that can be easily immersed in and extracted from reaction mixtures. The uniform tubular pores, falling within the mesoporous range, facilitate the smooth diffusion of reactants and products, which makes AAO a potential candidate for catalyst support [2, 23]. Ni-based catalysts were found to be very active for the

reaction in the work of M.N Gebresillase et al. [13]. This research team reported that [2:1] Ni-Cu/Al<sub>2</sub>O<sub>3</sub> catalyst was 100.0% to  $\lambda$ -valerolactone of levulinic acid with >99.0% selectivity, and [2:1] Ni-Co/Al<sub>2</sub>O<sub>3</sub> was 83.0% selectivity to  $\lambda$ -valerolactone of levulinic acid found a conversion rate of 100.0%. In another study [24, 25], the catalytic properties of aluminum oxide were also studied in the conversion reactions of isopropyl alcohol. According to the results, it was found that the introduction of heteropolyacid into  $\gamma$ -Al<sub>2</sub>O<sub>3</sub> increases the conversion level by 1.5 times, while its introduction into  $\eta$ -Al<sub>2</sub>O<sub>3</sub>, on the contrary, reduces the conversion level by 10%.

In the works of A.Sh. Aliyev and et al. [26] the deposition of CdS using cadmium ions on a nickel electrode was studied. The results of the study made it possible to determine the potential range at which the deposition of cadmium with sulfur occurs, as well as the influence of the composition of the electrolyte and electrolysis conditions on the process.

In this section, we focused on evaluating the activity of nickel and bimetallic (nickel and molybdenum) nanocomposites in the hydrogenation of unsaturated hydrocarbons at various temperatures. Nanoparticles were prepared by impregnating nickel and nickel-molybdenum on the surface and into the pores of AAO. The catalyst was subsequently evaluated for its effectiveness in converting hexene to hexane. The mass of the nickel nanoparticles deposited on an inert AAO substrate was about 21 wt%. The catalyst was loaded into a flow-type reactor in a wet state and then dried in a stream of hydrogen at 250-300 °C for 30 minutes. In the reactor, a catalyst layer was positioned between

inert silica glass packing layers. Following the drying process, unsaturated compound and hydrogen were introduced directly to the catalyst from top to bottom at appropriate temperatures. Hydrogenation was carried out for 2-12 hours at 200 °C, 250 °C, 300 °C and 350 °C under a pressure of 1 atm. The hydrogenation process conditions and the results comparison with a conventional Ni/SiO<sub>2</sub>-containing catalyst are presented in Table 1.

700 III 4	T .	1 1	C	•	, C1
I ahie i	Lemnerature	denendence	ot con	Version	rate of hexane
I abic I	1 Chipciatuic	acpenache		VCISIOII	rate or nexame

	H <sub>2</sub> flow rate -1000 ml/h, pressure 1 atm					
Catalyst	Hexane conversion rate; %					
	200°C	250°C	300°C	350°C		
Ni/AAO	32	45	73	90		
Ni/SiO <sub>2</sub>	-	39	60	78		

The data in Table 1 indicates that the conventional Ni/SiO<sub>2</sub>-containing catalyst showed no activity at 200 °C and its catalytic activity was only observed at temperatures above 250 °C. Furthermore, the catalyst's activity increased with the rise in temperature during the

hydrogenation of hexene. The mixture of gases passing through the catalytic system during the hexene-hexane hydrogenation was analyzed chromatographically, and the results are depicted in Figs. 6 and 7.

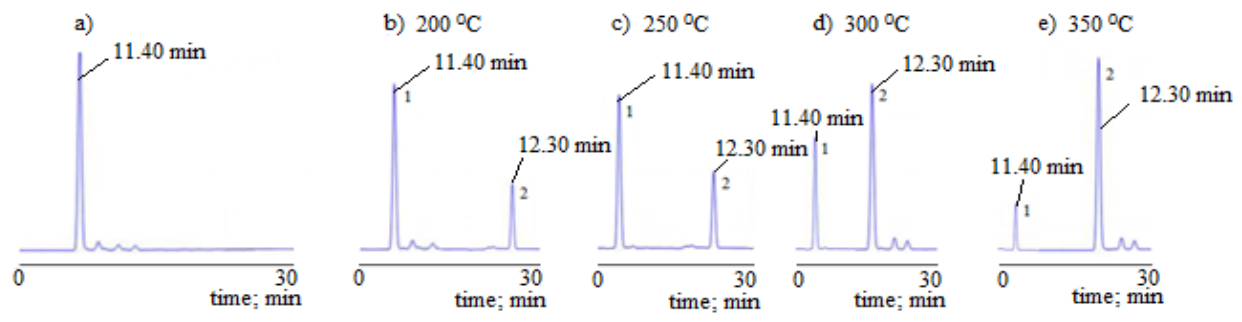


**Fig. 6.** Ni/AAO-containing catalyst conversion of Hexene- (a) and a mixture of hexane-hexene (be) chromatograms. Hexene and hexane peaks are denoted by numbers 1 and 2 accordingly.

A chromatogram of hexane-1 was obtained to determine the conversion rate of hexane. Since, hexane-1 is chemically pure (99%), chromatography revealed only one distinct peak, observed at 11.40 minutes as shown in Fig. 6a. However, with the synthesized Ni/AAO-containing catalyst, the conversion of hexane was 32% at 200 °C (Fig. 6b), and it increased with rising temperatures - reaching 45% at 250 °C (Fig. 6c), 73% at 300 °C (Fig. 6d), and 90% at 350 °C (Fig. 6e). There was only a marginal increase in conversion rates (1-2%) at higher temperatures.

Hexene-hexane hydrogenation was also carried out in the presence of a catalyst containing Ni-Mo/AAO. To do this, the catalyst

was placed into a catalytic column in a layer-bylayer manner with silicates. A mixture of hexene and hydrogen gases was passed from top to bottom through the catalytic reactor. The chromatographic analysis results of the of the gas mixture flowing through the catalytic column are shown in Fig. 7.

Similarly, the Ni-Mo/AAO catalyst did not show activity at 200 °C (Fig. 7a) but became active at 250 °C, achieving a hexane conversion rate of 41% (Fig. 7b). The conversion rate further increased to 69% at 300 °C (Fig. 7c) and 84% at 350 °C (Fig. 7d). As observed with the Ni/AAO catalyst, there was a slight increase (1-2%) in conversion rate at temperatures above 400 °C. The results of the chromatographic analysis

indicate that the hexane-hexene conversion rate also rose with increasing temperature during the hydrogenation of hexene. Details of the hydrogenation process are provided in Table 2.

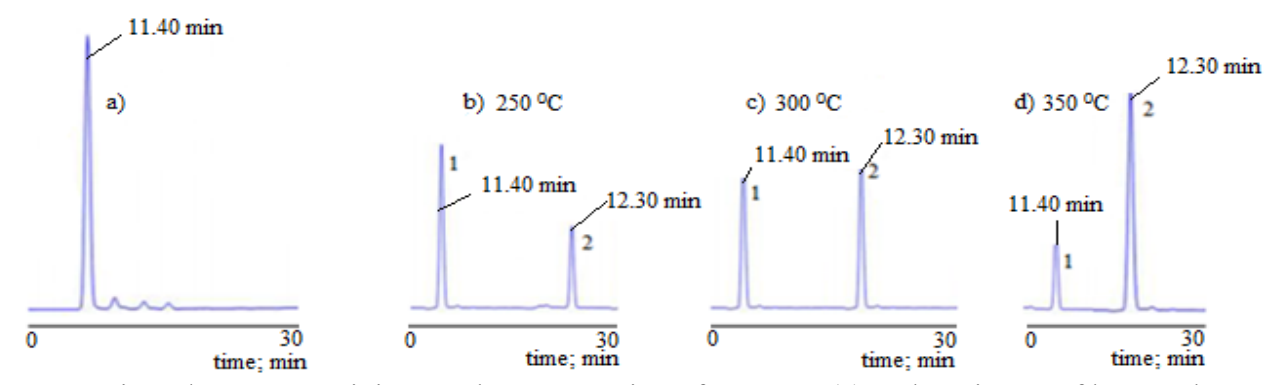


**Fig. 7.** Ni-Mo/AAO -containing catalyst conversion of Hexene- (a) and a mixture of hexane-hexene (b-d) chromatograms. Hexene and hexane peaks denoted by numbers 1 and 2 accordingly.

The catalytic activity of the porous nanostructured Ni/AAO and Ni-Mo/AAO catalysts in the process of hydrogenation of other unsaturated hydrocarbons as a function of

temperature is summarized in Table 2. It was found that the conversion rate of the product increased proportionally with rising temperatures.

**Table 2.** Temperature dependence of conversion rate at hydrogen flow rate - 1000 ml/h, and pressure of 1 atm.

Alkene→Alkane	Conversion rate, %.							
AIRCIIC / AIRAIIC	200°C	250°C	300°C	350°C				
Ni/AAO								
C <sub>6</sub> H <sub>12</sub> →C <sub>6</sub> H <sub>14</sub>	32	45	73	90				
C7H14→C7H16	29	40	68	85				
$C_8H_{16}\rightarrow C_8H_{18}$	24	37	66	82				
Ni-Mo/AAO								
$C_6H_{12}\rightarrow C_6H_{14}$	-	40	69	84				
C7H14→C7H16	-	37	67	81				
C <sub>8</sub> H <sub>16</sub> →C <sub>8</sub> H <sub>18</sub>	-	32	61	74				

Furthermore, it was observed that the conversion rate decreased with an increase in the molecular weight of unsaturated hydrocarbons (C6 to C8) when using the Ni/AAO catalyst. Conversely, the Ni-Mo/AAO catalyst showed activity at 250 °C for all unsaturated

hydrocarbons but displayed a decreasing conversion rate from C6 to C8. Overall, the Ni/AAO catalyst demonstrated its highest catalytic activity at 200 °C and proved to be the most effective catalyst for hydrogenation processes.

#### Conclusion

Nanostructured anodic aluminum oxide membranes were successfully synthesized using commercial aluminum film and their characteristics were systematically studied by varying the oxalic acid temperature. These AAO membranes presented a short-range pore arrangement, with changes in pore diameters and interpore distances primarily influenced by the

anodizing temperature. Catalytic testing demonstrated the efficacy of the Ni/AAO catalyst in hydrocarbon conversion reactions, highlighting its potential to use various oil refining processes. The findings of this study hold practical significance in the field of catalyst development for processes such as cracking, isomerization, and aromatization of n-paraffins.

## **Declaration of Competing Interest**

The authors declare that they have no known competing financial interests or personal relationships that could have appeared to influence the work reported in this paper.

## Acknowledgements

This research was financially supported by Ministry of Innovative Development of the Republic of Uzbekistan (Project #: MUK-2021-45) and Key Special Projects of the Ministry of Science and Technology, China (Project #: 2021YFE0104300).

#### References

- 1. Fernández-Romero L., Montero-Moreno J.M., Pellicer E., Peiro F., Cornet A., Morantea J.R., Sarret M., Muller C. Assessment of the thermal stability of anodic alumina membranes at high temperatures. *Materials Chemistry and Physics*, 2008, **Vol. 111**, p. 542-547. DOI: https://doi.org/10.1016/j.matchemphys.2008. 05.003
- 2. Crouse D., Lo Yu-H., Miller A.E., Crouse M. Self-ordered pore structure of anodized aluminum on silicon and pattern transfer. *Applied Physics Letters*, 2000, **Vol. 76**, p. 49-51. DOI: https://doi.org/10.1063/1.125652
- 3. Tomassi P., Buczko Z. Aluminum anodic oxide AAO as a template for formation of metal nanostructures. *Electroplating of Nanostructures*. 2015. Chapter. 318 p. DOI: https://doi.org/10.5772/61263
- 4. Jai Poinern G.E., Ali N., Fawcett D. Progress in nano-engineered anodic aluminum oxide membrane development. *Materials*, 2011, **Vol.** 4(3), p. 487-526. DOI: https://doi.org/10.3390/ma4030487
- 5. Jai Poinern G.E., Brundavanam R.K., Le X.T., Nicholls P.K., Cake M.A., Fawcett D. The synthesis, characterisation and *in vivo* study of a bioceramic for potential tissue regeneration applications. *Scientific Reports*, 2014, **Vol. 4(1)**, p. 6235. DOI: https://doi.org/10.1038/srep06235
- 6. Bruera F.A., Kramer G.R., Vera M.L., Ares A.E. Synthesis and morphological characterization of nanoporous aluminum oxide films by using a single anodization step. *Coatings*, 2019, **Vol. 9(2)**, p. 115 A. doi: https://doi.org/10.3390/coatings9020115
- 7. Wlodarczyk-Fligier A., Labizs K. Influence of aluminium alloy anodizing and casting methods on structure and functional properties. *Archives of Metallurgy and Materials*, 2016, Vol. 61(3), p. 991–96. DOI:

### https://doi.org/10.1515/amm-2016-0220

- 8. Mozalev A. Anodic film growth on Al layers and Ta-Al metal bilayers in citric acid electrolytes. *Electrochimica Acta*, 2005, **Vol. 50(25-26)**, p. 5065-5075. DOI: https://doi.org/10.1016/j.electacta.2005.02.09
- Chernyakova K., Tzaneva B., Vrublevsky I., Videkov V. Effect of aluminum anode temperature on growth rate and structure of nanoporous anodic alumina. *Journal of The Electrochemical Society*, 2020, Vol. 167, 103506. DOI: https://doi.org/10.1149/1945-7111/ab9d65
- 10. Khamidov A., Ibragimova I., Mirxamitova D., Nurmanov S., Ruzimuradov O. Morphological properties of anodic aluminum oxide membrane synthesized as an electrolyte in oxalic acid. *ACTA NUUz*, 2022, **Vol. 3(1)**, p. 340-344. DOI: https://doi.org/10.31618/nas.2413-5291.2020.2.60.303
- 11. Cheng T.C., Chou C.C. The electrical and mechanical properties of porous anodic 6061-T6 aluminum alloy oxide film. *Journal of Nanomaterials*, 2015, **Vol. 1**, p. 128-132. DOI: https://doi.org/10.1155/2015/371405
- 12. Butanov Kh., Hoshimov F., Khamidov A., Mamatkulov Sh., Fang D., Ruzimuradov O. Pressure driven growth of In-Sn alloy nanowires in anodic aluminum oxide nanochannel: simulation and experimental study. *Bulletin of Chemical Reaction Engineering & Catalysis*, 2020, **Vol. 15**, p. 3. DOI: https://doi.org/10.2139/ssrn.4526435
- 13. Gebresillase M.N., Raguindin R.Q., Kim H., Seo J.G. Supported bimetallic catalysts for the solvent-free hydrogenation of levulinic acid to -valerolactone: effect of metal combination (Ni-Cu, Ni-Co, Cu-Co).

- *Catalysts*, 2020, **Vol. 10(11)**, p. 1354-1359. DOI: https://doi.org/10.3390/catal10111354
- 14. Ayalew A.A., Han X., Sakairi M. Effect of substrate temperature and electrolyte composition on the fabrication of throughhole porous AAO membrane with SF-MDC. *Materials Chemistry and Physics*, 2024, Vol. 323(2), p. 15-25. DOI: 10.1016/j.matchemphys.2024.129658
- 15. Sulka G.D., Parkoła K.G. Anodising potential influence on well-ordered nanostructures formed by anodisation of aluminium in sulphuric acid. *Thin Solid Films*, 2006, **Vol. 515(1)**, p. 338-45. DOI: https://doi.org/10.1016/j.tsf.2005.12.094
- 16. Stępniowski W.J., Bojar Z. Synthesis of anodic aluminum oxide (AAO) at relatively high temperatures. Study of the influence of anodization conditions on the alumina structural features. Surface and Coatings technology, 2011, Vol. 206(2-3), p. 265-272. DOI: https://doi.org/10.1016/j.surfcoat.2011.07.0
- 17. Ku Ch.-A., Yu Ch.-Y., Hung Ch.-W., Chung Ch.-K. Advances in the fabrication of nanoporous anodic aluminum oxide and its applications to sensors: A review. *Nanomaterials*, 2023, Vol. 13(21), p. 2853. DOI: https://doi.org/10.3390/nano13212853
- 18. Vojkuvka L., Marsal L.F., Ferré-Borrull J., Formentin P., Pallarés J. Self-ordered porous alumina membranes with large lattice constant fabricated by hard anodization. *Superlattices and Microstructures*, 2008, Vol. 44(4-5), p. 577-582. DOI: https://doi.org/10.1016/j.spmi.2007.10.005
- 19. Nielsch K., Choi J., Schwirn K., Wehrspohn R.B., Gösele U. Self-ordering regimes of porous alumina: the 10 porosity rule. *Nano Letters*, 2002, **Vol. 2(7)**, p. 677-680. DOI: https://doi.org/10.1021/nl025537k
- 20. Hwang S.K., Jeong S-H., Hwang H-Y., Lee O-J., Lee K-H. Fabrication of highly ordered

- pore array in anodic aluminum oxide. *Korean Journal Chemical Engineering*, 2002, **Vol. 19**, p. 467-73. DOI: https://doi.org/10.1007/BF02697158
- 21. Ateş S., Baran E., Yazıcı B. The nanoporous anodic alumina oxide formed by two-step anodization. *Thin Solid Films*, 2018, **Vol. 648**, p. 94-102. DOI: https://doi.org/10.1016/j.tsf.2018.01.013
- 22. Kozhukhova A.E., du Preez S.P., Bessarabov D.G. Preparation of anodized aluminium oxide at high temperatures using low purity aluminium (Al6082) // Surface & Coatings Technology, 2019, pp. 378. doi: https://doi.org/10.1016/j.surfcoat.2019.1249 70
- 23. Eessaa A.K., El-Shamy A.M. Review on fabrication, characterization, and applications of porous anodic aluminum oxide films with tunable pore sizes for emerging technologies. *Microelectronic Engineering*, 2023, **Vol. 279**, 112061. DOI: https://doi.org/10.1016/j.mee.2023.112061
- 24. Kim J., Jeong Ch. Research on variation in nanopore parameters and surface characteristics of anodic aluminum oxide (AAO) films with time-controlled anodization processes. *Journal of Materials Science*, 2024, Vol. 59(23), p. 10556-10571. DOI: https://doi.org/10.1007/s10853-024-09806-y
- 25. Yusubova S.E., Huseynova E.A., Ajamov K.Yu. Catalytic activity of heteropoly acid-containing aluminum oxide in the reactions of isopropyal alcohol conversion. *Chemical problems*, 2018, **Vol. 16(1)**, p. 127-135.
- 26. Aliyev A.Sh., Eminov Sh.O., Soltanova T.Sh., Mejidzadeh V.A., Kuliyev D.A., Jalilova H.D., Tagiyev B. Electrochemical production of thin films of cadmium sulphide on nickel electrodes and research into their morphology. *Chemical problems*, 2016, **no. 2**, p. 139-145.